Anal. Chem. **1999,** *71,* 4385−4391

Mapping of Platinum Group Metals in Automotive Exhaust Three-Way Catalysts Using Laser-Induced Breakdown Spectrometry

Patricia Lucena, José M. Vadillo, and J. Javier Laserna*

Department of Analytical Chemistry, Faculty of Sciences, University of Málaga, E29071 Málaga, Spain

The use of laser-induced breakdown spectrometry for spatial distribution analysis of platinum, rhodium, and palladium in car catalytic converters is discussed. Fresh converters were extracted from the car exhaust system, cut in pieces of an appropriate size, and analyzed for mapping purposes. Spectral detection, pulse energy, and beam focal conditions were optimized according to the ablation behavior of the material. Difficulties in distribution analysis caused by the complex elemental composition of the sample were overcome by an extensive spectral analysis using appropriate internal standards. Data on the spatial distribution of the active metals in both the axial and radial directions of the catalytic structures are presented.

The use of catalytic converters for the purification of automotive exhaust gases is today a general practice in industrialized countries in an attempt to maintain the car exhaust emissions at acceptable levels. Catalytic converters are incorporated into the exhaust system in automobiles to promote mainly three different reactions: reduction of NO_x to nitrogen and water, oxidation of carbon monoxide to carbon dioxide, and finally to complete the combustion (oxidation) of residual hydrocarbons.[1−3] As the conversion of the three pollutant groups is carried out at the same time, such type of converter is usually called a three-way catalyst (TWC). The most frequently used TWCs consist of an alumina-coated ceramic structure supporting the platinum group metals (PGM) in charge of the catalytic action insulated by a Teflon cover and enclosed in a stainless steel casing. This casing directs the exhaust gas flow through channels in the catalyst bed. The ceramic structure is a monolithic support of cordierite ($2MgO{\cdot}2Al_2O_3{\cdot}5SiO_2$). The ceramic is coated with γ-alumina where the PGMs are incorporated. This alumina layer containing the PGM is called the washcoat and usually embodies other elements such as Zr, Ce, La, and others, depending on the manufacturer. The active catalyst elements are platinum and/or palladium used for hydrocarbon and CO oxidation and rhodium used for NO_x reduction.

Although the great advantages of autocatalysts are obvious, there are however some disadvantages in their usage. The most important concern is the release of PGMs to the environment as a result of surface abrasion of the catalytic converters during car operation. Catalytic converters are nowadays considered to be the prime source for the highly elevated platinum concentrations observed recently in samples taken in heavy traffic areas. Lustig reported[4] that the Pt concentration in samples of sediments, dusts, and plants near highways in Austria, Belgium, Sweden, Germany, and the United Kingdom has increased by 3−6 orders of magnitude in the last 10 years. The possible health effects of increasing Pt concentrations in urban road dust and soil and in blood and urine were discussed by Farago et al.[5] Analysis was performed by inductively coupled plasma mass spectrometry (ICPMS). Metallic Pt is considered to be biologically inert and nonallergenic, and since the emitted Pt is probably in the metallic or oxide form, the sensitizing potential is probably very low. However, Pt from road dust can be solubilized and enter waters, sediments, soils, and the food chain.[5] Krachler and co-workers monitored the catalytic active components in human urine by quadrupole and magnetic sector field ICPMS.[6] The study was conducted with youngsters, and the findings allow the Pt levels of these subjects to be defined at or below 1 ng L^{-1} and the Pd and Rh contents at ∼10 ng L^{-1}.

Stembon reported[7] that loss of PGM material is one of the several processes causing catalyst deactivation during car operation. Thus, an approach to understand the processes leading to the release of PGM to the environment is to study the catalyst surface and to determine the PGM concentration before and after car operation for an extended period of time. In principle, analytical information should be provided with a reasonable degree of spatial localization to gain in the understanding of the catalyst function as a whole. Techniques used in the analysis of automobile catalysts include inductively coupled plasma mass spectrometry with spark ablation (SA-ICPMS),[8] inductively coupled plasma mass spec-

(1) Kallmann S.; Blumberg, D. *Talanta* **1980**, 827−833.
(2) Taylor, K. C. In *Automobile Catalytic Converters*; Taylor, K. C., Ed.; Springer-Verlag: Berlin, 1984.
(3) Koltsakis, G. C.; Stamatelos, A. M. *Prog. Energy Combust.* Sci. **1997**, *23*, 1−39.
(4) Lustig, S. In *Platinum in the Environment*; Lustig, S., Ed.; Herbert Utz Verlag Wissenschaft: München, 1997; pp 1−25.
(5) Farago, M. E.; Kavanagh, P.; Blanks, R.; Kelly, J.; Kazantzis, G.; Thornton, I.; Simpson, P. R.; Cook, J. M.; Delves, H. T., Gwendy, E. M. *Analyst* **1998**, *123*, 451−454.
(6) Krachler, M.; Alimonti, A.; Petrucci, F.; Irgolic, K. J.; Forastiere, F.; Caroly, S. *Anal. Chim. Acta* **1998**, *363*, 1−10.
(7) Stenbom, B. In *Microstructural Changes in Deactivivated Noble Metal Catalysts*; Stenbom, B., Ed.; Department of Physics: Goteborg, 1994; pp 1−7.
(8) Borisov, O. V.; Coleman, D. M.; Carter, R. O. *J. Anal. Atom. Spectrom.* **1997**, *12*, 231−237.

10.1021/ac9902998 CCC: $18.00
Published on Web 09/03/1999

trometry with liquid nebulization (LN-ICPMS),[9] glow-discharge mass spectrometry (GD-MS),[10] glow-discharge atomization atomic absorption spectrophotometry (GDA-AAS),[11] and electrothermal atomization laser-excited atomic fluorescence (EA-LEAF).[12] All these techniques have difficulties with the extensive treatment needed for sample dissolution or, for techniques working directly with the solid, with the nonconducting properties of the catalyst surface. In addition, these approaches are not suited for distribution analysis of the PGM in the catalytic converters. Several surface analysis techniques have been used for examining the catalyst surface, including transmission electron microscopy, X-ray diffraction, X-ray photoelectron spectroscopy, and low-energy ion scattering spectroscopy.[13] However, when one tries to characterize large catalyst structures such as catalytic converters, these techniques are not practical because of several experimental problems due to the extensive sample preparation needed, to the small sampling areas examined, and to the difficulties with handling large samples in high-vacuum environments.

The capability of laser-induced breakdown spectrometry (LIBS) for materials characterization has been widely demonstrated. Although laser ablation can be performed for any types of sample,[14−16] LIBS has found the most widespread use in the analysis of solid materials.[17−20] Most applications of LIBS have so far concentrated on specimens where the concentration is uniform over the analyzed volume. However, spatial localization is an inherent attribute of LIBS as usually the laser is focused at the sample surface to obtain the beam irradiance required for ablation and plasma formation. By translating the sample position under the laser beam, so that the analyzed region is moved across the static laser beam, lateral profiles of the sample constituents can be readily obtained. Also, a depth profile of a sample may be obtained simply by acquiring sequential LIBS spectra as the surface is ablated shot-by-shot by the incident laser beam. Both acquisition modes have been used with success for laterally inhomogeneous surfaces[21,22] and for samples showing variations in concentration with depth.[23−26] Typical dimensions involved in LIBS are in the micrometer scale, although depth resolution in the nanometric range has been documented for coated steels.[27] By combining lateral imaging with depth profiling, three-dimensional compositional maps can be developed through the use of computer-assisted imaging to reconstruct desired cross-sectional views of the specimen from a series of lateral images taken as a function of depth. The so-called imaging-mode LIBS has been developed[28,29] and used recently to describe the distribution of impurities in silicon,[30,31] for the analysis of element distribution in rocks,[32] and for imaging of copper in a printed circuit board.[33]

In this paper, research results obtained in the analysis of a fresh gasoline catalytic converter using LIBS are summarized. Following a study of the best experimental conditions for detection of Pt, Pd, and Rh in the converter, a distribution analysis of the elements of interest in the catalytic structure is described. Channel-to-channel compositional variability and differences of component distribution in the gas flow direction have been observed.

EXPERIMENTAL SECTION

A pulsed Nd:YAG laser (Continuum, model Surelite SLI-20, pulse width 5 ns) operating at the second harmonic wavelength of 532 nm was used to generate the microplasma in air at atmospheric pressure. An optical system guided the desired laser beam at normal incidence to the sample surface. The focusing lens, with a focal length of 100 mm and *f* number of 4, was mounted on a vertical translation stage so that the lens−target distance could be changed. The laser pulse energy was varied by changing the delay of the Q switch and was measured with a pyroelectric joulemeter (Gentec, model ED-200, with a nominal sensitivity of 9.86 V J^{-1}) coupled to a digital oscilloscope.

Laser-ablated plasma emission was collected by a planoconvex quartz lens (focal length 100 mm and *f* number 4) onto the entrance slit (10 μm wide and 10 mm high) of a 0.5-m focal-length Czerny-Turner spectrograph (Chromex, model 500 IS, with three indexable gratings of 300, 1200, and 2400 grooves mm^{-1}). Light was dispersed using the 2400 grooves mm^{-1} grating, and the reciprocal linear dispersion was 2.5 nm mm^{-1}. The spectral resolution of the system was 0.02 nm $pixel^{-1}$. The dispersed-plasma light was detected using a two-dimensional charge-coupled device (CCD) detector (Stanford Computer Optics, model 4Quik 05) equipped with an intensifier system. The CCD consists of 752-(h) × 582(v) elements. The photoactive area is 6 × 4.5 mm^2. These values gave a spectral coverage of ∼15 nm. Operation of the detector was controlled by 4 Spec 1.20 software. The emission signal was corrected by subtraction of the dark current of the detector, which was separately measured for the same exposure time. Each pulse was stored as a file containing spectral and spatial

(9) Borisov, O. V.; Coleman, D. M.; Oudsema, K. A.; Carter, R. O. *J. Anal. At. Spectrom.* **1997**, *12*, 239−246.
(10) Wayne, D. M. *J. Anal. At. Spectrom.* **1997**, *12*, 1195−1202.
(11) Winchester, M. R.; Hayes, S. M.; Marcus. R. K. *Spectrochim. Acta* **1991**, *46B*, 615−627.
(12) Aucelio, R. Q.; Rubin, V. N.; Smith, B. W.; Winefordner, J. D. *J. Anal. At. Spectrom.* **1998**, *13*, 49−54.
(13) Skoglundh, M.; Lowendahl, L. O.; Menon, P. G.; Stenbom, B. J. P.; Vankessel, O.; Brongersman, H. H. *Catal. Lett.* **1992**, *13*, 27−38.
(14) Williamson, C. K.; Daniel, R. G.; Mcnesby, K. L.; Miziolek, A. W. *Anal. Chem.* **1998**, *70*, 1186−1191.
(15) Neuhauser, R. E.; Panne, U.; Niessner, R.; Petrucci, G. A. *Anal. Chim. Acta* **1997**, *346*, 37−48.
(16) Arca, G.; Ciucci, A.; Palleschi, V.; Rastelli, S.; Tognoni, E. *Appl. Spectrosc.* **1991**, *51*, 1102−1105.
(17) Brian, J. M.; Scott, R. G.; Michael A. *Anal. Chem.* **1996**, *68*, 977−981.
(18) Hidalgo, M.; Martin, F.; Laserna, J. J. *Anal. Chem.* **1996,** *68*, 1095−1100.
(19) Eppler, A. S.; Cremers, D. A.; Hickmott, D. D.; Ferris, M. J. *Appl. Spectrosc.* **1996**, *50*, 1175−1181.
(20) Milán, M.; Lucena, P.; Cabalín, L. M.; Laserna, J. J. *Appl. Spectrosc.* **1998**, *52*, 444−448.
(21) Talmi, Y.; Sieper, H. P.; Moenke-Blakenburg, L. *Anal. Chim. Acta* **1981**, *127*, 71−85.
(22) Vadillo, J. M.; Vadillo, I., Carrasco, F.; Laserna, J. J. *Fresenius J. Anal. Chem.* **1998**, *361*, 119−123.
(23) Lorenzen, C. J.; Carlhoff, C.; Hahn, U.; Jogwich, M. *J. Anal. At. Spectrom.* **1992**, *7*, 1029−1035.
(24) Anderson, D. R.; Mcleod C. W.; English, T.; Smith, A. T. *Appl. Spectrosc.* **1995**, *49*, 691−701.
(25) Vadillo, J. M.; Laserna, J. J *J. Anal. At. Spectrom.* **1997**, *12*, 859−862.
(26) Häkkänen, H. J.; Korppi-Tomola, J. E. I. *Anal. Chem.* **1998**, *70*, 4724−4729.
(27) Vadillo, J. M.; Garcia, C.; Palanco, S.; Laserna, J. J. *J. Anal. At. Spectrom.* **1998**, *13*, 793−797.
(28) Häkkänen, H. J.; Korppi-Tomola, J. E. I. *Appl. Spectrosc.* **1995**, *49*, 1721−1728.
(29) Romero, D.; Laserna, J. J. *Anal. Chem.* **1997**, *69*, 2871−2876.
(30) Romero, D.; Laserna, J. J. *J. Anal. At. Spectrom.* **1998**, *13*, 557−560.
(31) Romero, D.; Fernández, J. M.; Laserna, J. J. *J. Anal. At. Spectrom.* **1999**, *14*, 199−204.
(32) Yoon, Y. Y.; Kim, T. S.; Chung, K. S.; Lee, K. Y.; Lee, G. H. *Analyst* **1997**, *122*, 1223−1227.
(33) Kim, T.; Lin, C, T. *J. Phys. Chem. B* **1998**, *102*, 4284−4287.

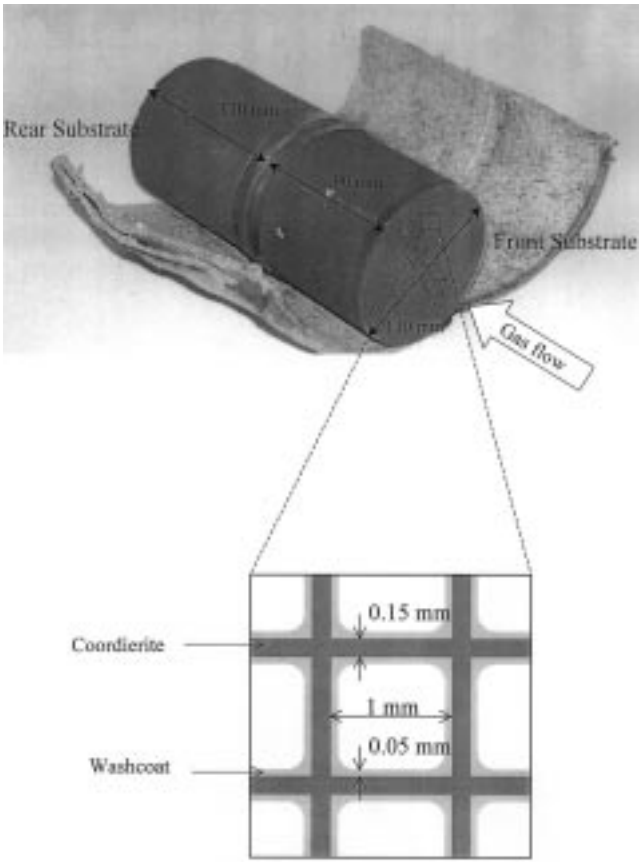

Figure 1. Photograph of a three way automotive catalyst, showing the casing of the converter. The inset shows a schematic diagram of the catalytic structure.

information. Spectral calibration was conducted by comparing the spectra from several pure metals in the same spectral window.

Samples were placed on a manual $x-y-z$ translation stage to be moved with respect to the laser beam. The converter analyzed in this report was provided by Ford España, S.A., and corresponds to a gasoline-fueled engine. The converter was made of monolithic structures of cordierite (62 cells/cm^2) and consisted of two parts, the front and the rear substrates. The front substrate contains only Pt and Rh and has a metal loading of 2119 g/m^3 with a weight ratio Pt/Rh = 9/1. The rear substrate contains Pd and Rh and had a weight ratio Pd/Rh = 9/1. A longitudinal cross section of the honeycomb structure analyzed by scanning electron microscopy (SEM) revealed the width of the channels to be 1 mm and the cordierite wall and washcoat thicknesses 150 and 50 μm, respectively. Figure 1 shows a photograph of the converter with a schematic diagram of the catalytic structure. The converter as received from the manufacturer was installed in the exhaust pipe, which was carefully opened to extract the intact catalytic structure. The converter was then cut in sections for analysis, with special care to avoid mechanical stress. Washcoat samples were taken from the cordierite walls by scraping with a brush. The washcoat powder was then homogeneized and ground in an agate mortar and pelletized in a press. This process ensured that the material would be homogeneous over the focused laser spot size when irradiated.

RESULTS AND DISCUSSION

Spectral Description of TWC. Several difficulties are associated with the local analysis of cordierite catalysts using optical emission spectrometry. First is the complex elemental composition of the washcoat, with many emission lines apart from those of the PGM. In particular, the presence of rare-earth elements (REEs) Fe and Zr makes it difficult to find spectral regions free from spectral interference. Second, the powdered nature of the washcoat dictates the use of high-energy laser pulses in order to result in breakdown of the ablated material. Under these circumstances, the spectra are composed mainly of emissions from both the washcoat and the cordierite matrix (mainly Si, Al, and Mg). And finally, the fast temporal decay of Pt emission, which demands prompt data acquisition after the laser pulse. Under these conditions, the spectra exhibit a large nonresonant background emission that masks the analyte signal. To deal with these problems, two different strategies were implemented

A systematic study was made of the optical emission spectra in selected regions of interest (ROIs) for each element. The ROIs for Pt, Pd, and Rh were 201−311, 220−380, and 230−370 nm, respectively. Two spectral windows were selected and used throughout. Figure 2 shows single-shot LIB spectra corresponding to the front and rear substrates in the Pt ROI, while Figure 3 shows the corresponding spectra in the Pd and Rh ROI. As shown, the spectra are quite crowded, with most lines corresponding to Ce, Fe, and Zr. In addition to the PGM lines, a Si line at 212.41 nm from the cordierite matrix and Ce and Zr lines at 222.10 and 339.20 nm, respectively, from the washcoat indicate that both structural components are being ablated and contribute to the observed spectra. The spectral features of the front and rear substrates confirm the compositional differences between both substrates. As shown in Figure 2a, the front substrate exhibits the Pt lines at 214.42 and 224.55 nm. However, there is no evidence of Pt in the rear washcoat (Figure 2b). Since the Pt (II) 224.55-nm line is interfered with, the Pt (I) line at 214.42 nm was used. Concerning Pd, the emission lines at 340.46, 342.12, and 343.35 nm were exhibited only by the rear substrate (Figure 3b), in good agreement with the expected structure. The strong contribution of Zr (II) at 340.48 nm prevents the use of the Pd line at 340.46 nm for analytical purposes. A comparison of parts a and b of Figure 3 indicates the presence of Rh in both front and rear substrates. The Rh (I) lines at 339.68 and 343.49 nm were used for spectral detection.

A second approach consisted of studying the effect of beam focal conditions on the PGM signal at different pulse energies. As the PGM information resides on the washcoat layer of the catalyst, increasing the surface sensitivity while maintaining a laser pulse energy exceeding the washcoat breakdown threshold is mandatory. However, because of the known variability of PGM distribution over the catalyst, a pilot study was conducted on pelletized washcoat samples taken from the catalyst. Figure 4 shows the results for Pt in a pellet made of the front washcoat. Focal conditions were modified by changing the focusing lens to sample distance (working distance, wd). The x-axis coordinate in Figure 4 at which the laser beam was focused at the surface is taken as zero (wd = 0). Negative values of wd refer to the beam focused at a position inside the material, while positive values of wd refer to the beam being focused at a distance above the sample

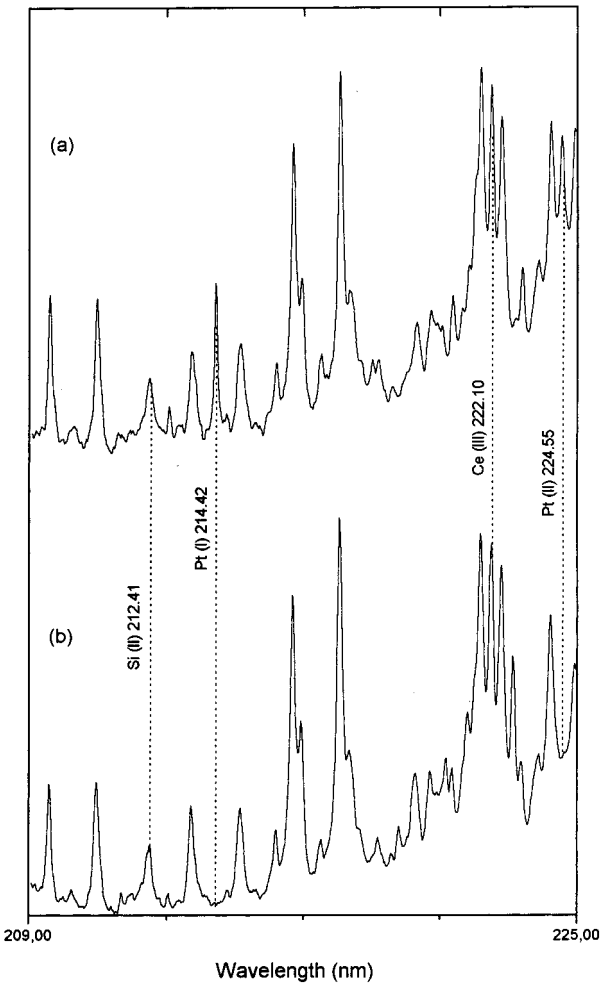

Figure 2. Single-shot LIB spectra from a fresh gasoline converter. (a) Front substrate containing Pt and Rh and (b) rear substrate containing Pd and Rh in the Pt spectral window. The delay time was 500 ns, and the acquisition time was 600 ns. The spectra correspond to the washcoat−cordierite interface. Pulse energy was 39.5 mJ.

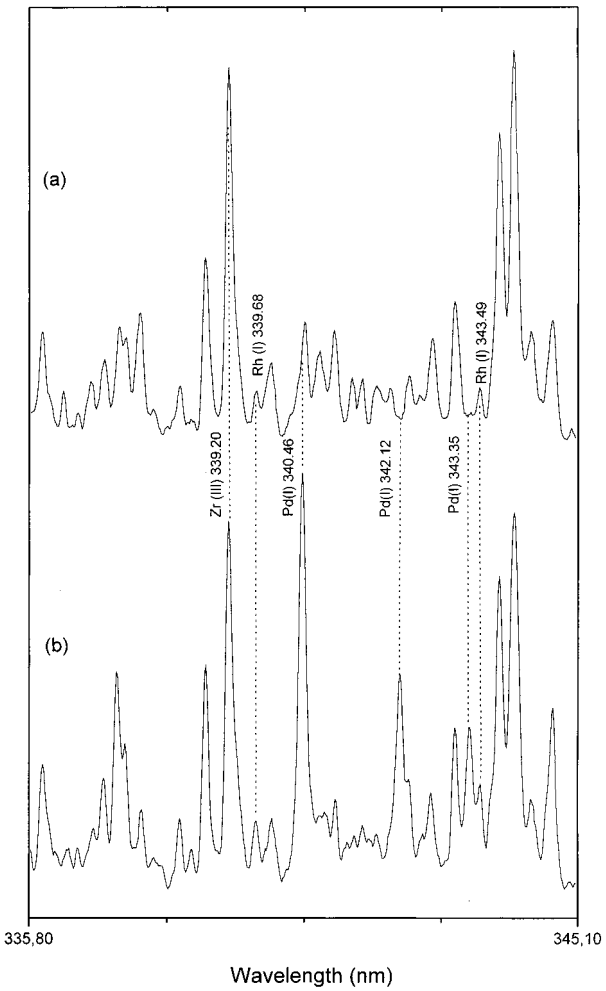

Figure 3. Single-shot LIB spectra from a fresh gasoline converter. (a) Front substrate containing Pt and Rh and (b) rear substrate containing Pd and Rh in the Pd−Rh spectral window. The delay time was 6 μs, and the acquisition time was 1 μs. The spectra correspond to the washcoat−cordierite interface. Pulse energy was 39.5 mJ.

surface. As shown, significant changes in Pt signal with both wd and pulse energy were observed. The largest signals were obtained by focusing the beam inside the material, with the maximum intensity observed at more negative wd values as the pulse energy is increased. Under these circumstances, the surface sensitivity in the LIBS analysis should be optimized at the expense of lateral resolution. However, the Pt signal cannot be increased indefinitely by working at more negative wd values and larger pulse energies since the maximum crater diameter allowed is limited by the channel size in the converter. At moderate pulse energies, a wd of −6 mm results in craters whose diameter is smaller than the 1-mm-wide channel walls (see Figure 1). Under these focal conditions, a study on the effect of pulse energy on Pt intensity was performed. The results are shown in Figure 5. The signal increased with energy with saturation above 40 mJ being observed due to plasma shielding by the vapor formed in front of the sample. A pulse energy of ∼40 mJ produces craters whose diameter is within the channel edges. This pulse energy was used in the converter analysis.

To verify that the signals acquired corresponded only to the washcoat layer of the converter, the Pt signal was monitored vs the number of laser shots in a single catalyst position together

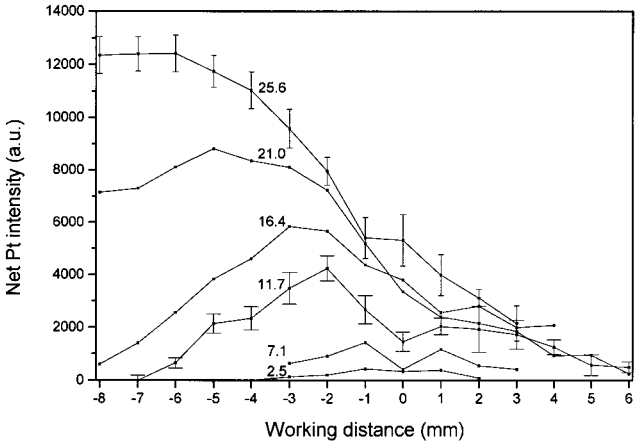

Figure 4. Net Pt intensity vs working distance at different pulse energies (mJ). Variation bars correspond to the range of five measurements in a pellet made of the front washcoat. The delay time was 500 ns, and the acquisition time was 600 ns.

with specific signals from the cordierite matrix. Figure 6 shows the depth profiles derived from the Pt (I) 214.42-nm and Si (I) 212.41-nm lines. Data points represent an average of seven measurements each on a fresh sample location in the front

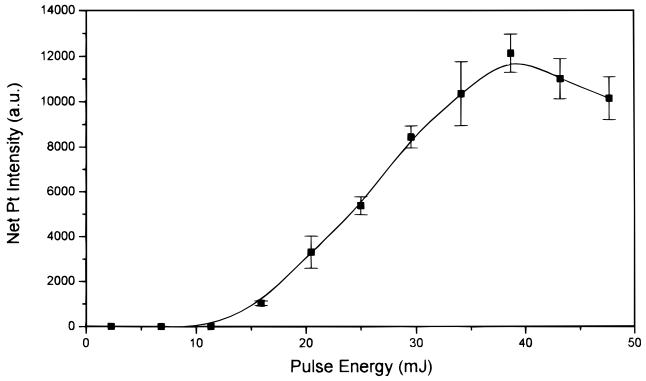

Figure 5. The Pt (I) 212.42-nm line behavior as a function of the laser pulse energy at a fixed working distance of −6 mm. The delay time was 500 ns, and the acquisition time was 600 ns.

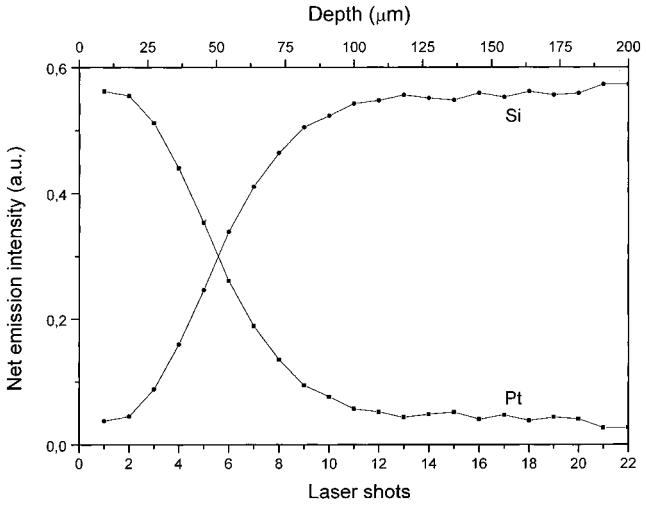

Figure 6. Emission intensity vs the number of laser shots of the Pt (I) 214.42-nm and Si (I) 212.41-nm spectral lines. Each curve represents an average of seven depth profiles in different sample locations. The approximate depth involved is displayed as an additional abscissa axis.

substrate of the converter. As shown, the depth profile confirms the presence of Pt on the surface of the front substrate, while the cordierite matrix appears as the washcoat is eroded. An axis indicating the depth involved is also included. To convert the laser shots axis into sample depth, an approximate ablation depth per laser shot (ad, μm pulse^{-1}) was calculated by dividing the wall thickness (as measured by scanning electron microscopy) by the number of laser shots just needed to drill the sample. Figure 7 shows a Rutherford backscattering micrograph of the catalyst showing the thickness associated with both the washcoat and the cordierite wall. The calculated ad value was 9.1 μm pulse^{-1} and was used in Figure 6. This conversion factor should be considered only as approximate, as the ablation depth per shot should not be identical for the washcoat and the cordierite matrix. Also, the ad is not expected to be linear. However, the calculated conversion factor will suffice for comparative purposes.

Spatial Distribution of PGM Constituents. To check for the compositional homogeneity of the converter, three sampling positions were selected along the longitudinal axis in both the front and rear substrates. Several channels at equivalent longitudinal positions were sampled and a fixed longitudinal position for each channel was analyzed to assess for compositional variability

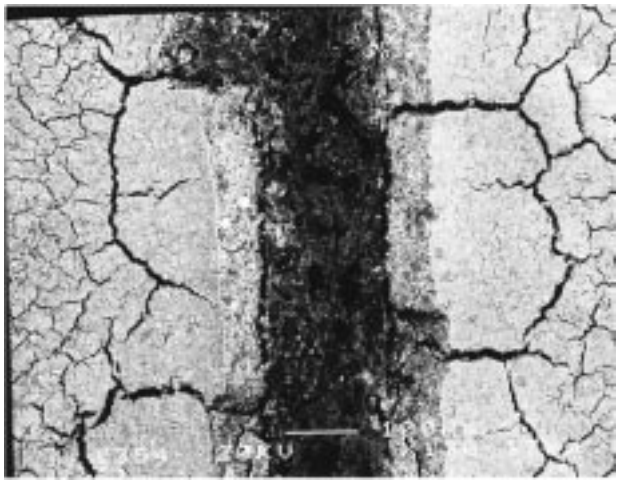

Figure 7. Rutherford backscattering micrograph of the three-way catalyst. The washcoat and cordierite relative compositions are shown as a function of the atomic number. The dark area in the center corresponds to the cordierite wall, while the bright area corresponds to the washcoat.

in the radial direction. As the Pt and Rh lines of interest are located in different ROI, alternate channels for each particular atomic species in the front substrate were analyzed. However, simultaneous Pd and Rh mapping in the rear substrate is possible since both elements exhibit their analytical lines in the same ROI. To compensate for shot-to-shot intensity variability, the ratios of the absolute intensities of the three PGMs to those of selected internal standards (Ce and Zr) present in the washcoat were determined. However, since the spatial distribution of Ce and Zr cannot be assumed to be uniform, the internal standard's homogeneity was evaluated. For that purpose, it was determined that aluminum was distributed homogeneously as this element is a major component of the washcoat. Unfortunately, aluminum could not be used as internal standard as it shows no sensitive emission lines in the Pt and Pd−Rh ROIs. The Ce/Al and Zr/Al intensity ratios in the selected sampling locations exhibit relative standard deviation values below 7%, which are compatible with the precision expected in LIBS. Thus, Ce and Zr can be considered to be homogeneously distributed, at least to the level of signal variability observed in LIBS. The Pt (I) 214.42/Ce (III) 222.10, Rh (I) 343.49/Zr (I) 339.20, Pd (I) 342.12/Zr (II) 339.20, and Rh (I) 339.68/Zr (II) 339.20 intensity ratios were used for mapping the Pt and Rh distributions in the front substrate and for Pd and Rh in the rear substrate, respectively. Figure 8 shows the results for the three elements. The inset in panel a shows a photomicrograph of the catalyst structure after laser ablation and analysis. The intensity matrixes obtained by LIBS mapping were manipulated for display purposes by a simple processing algorithm that involved assigning the gray scale to the data such that the zero is offset, and the threshold for gray is set to a given value, while the remaining values span the complete gray scale intensity range of the display. As shown, it is apparent that the distribution of the elements in the fresh converter analyzed is not uniform. The heterogeneity seems to be larger for Pt and Pd (Figure 8a) than for Rh (Figure 8b). Furthermore, the concentration variability appears in the longitudinal direction preferably as shown in the lateral profiles of Figure 9. The Pt and Pd contents seem to increase along the longitudinal axis, i.e., in the direction of the gas flow (Figure 9a

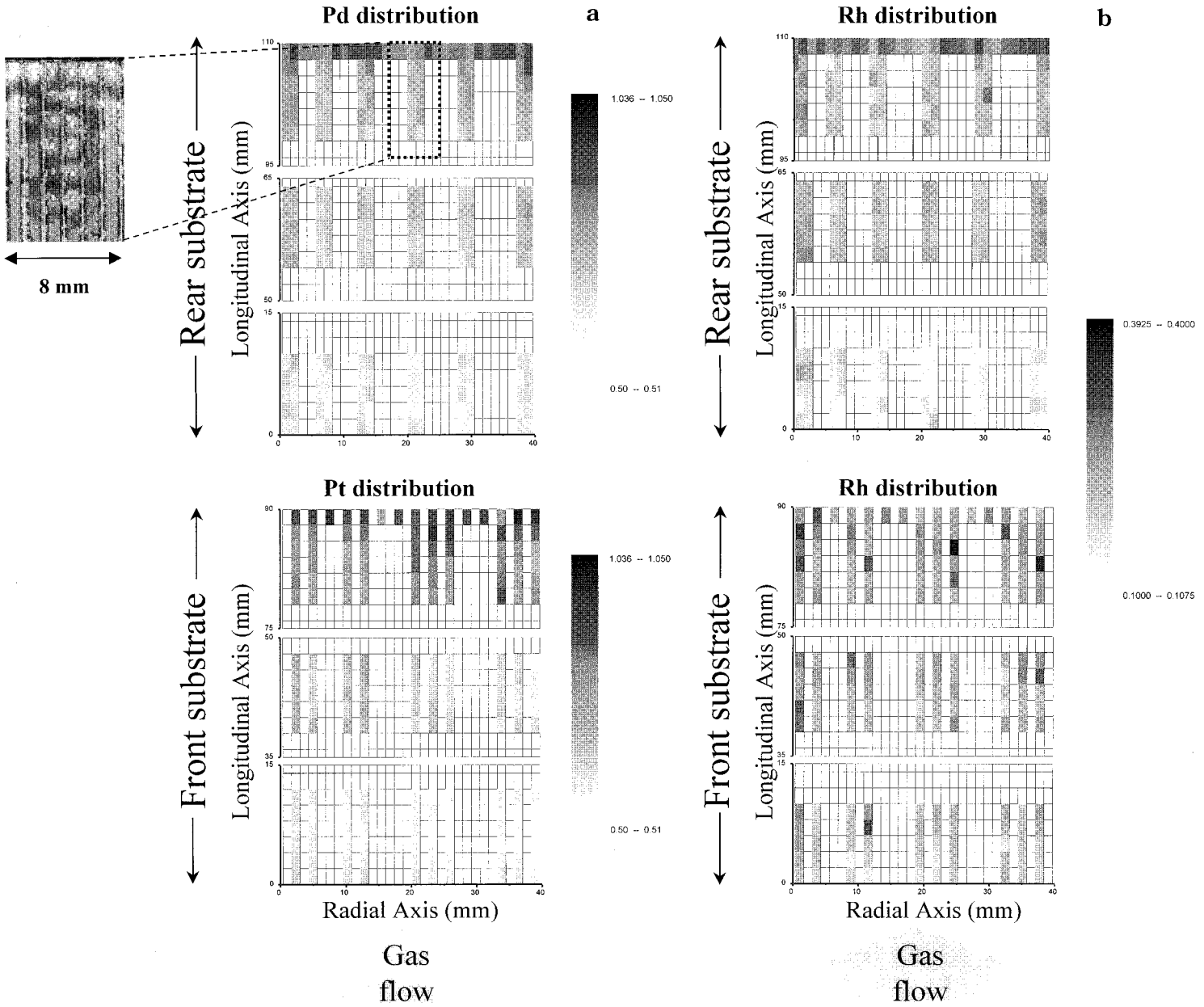

Figure 8. Distribution maps of Pt, Pd, and Rh in the front and rear substrates of a fresh catalytic converter. The Pt (I) 214.42/Ce (III) 222.10, Rh (I) 343.49/Zr(I) 339.20, Pd (I) 342.12/Zr (II) 339.20, and Rh (I) 339.68/Zr(II) 339.20 intensity ratios were used for mapping the Pt and Rh distributions in the front substrate and for Pd and Rh in the rear substrate, respectively. Panel a shows the Pd and Pt distributions and panel b shows Rh distributions. The inset represents a photomicrograph of part of the analyzed area, showing the ablation craters formed on the washcoat.

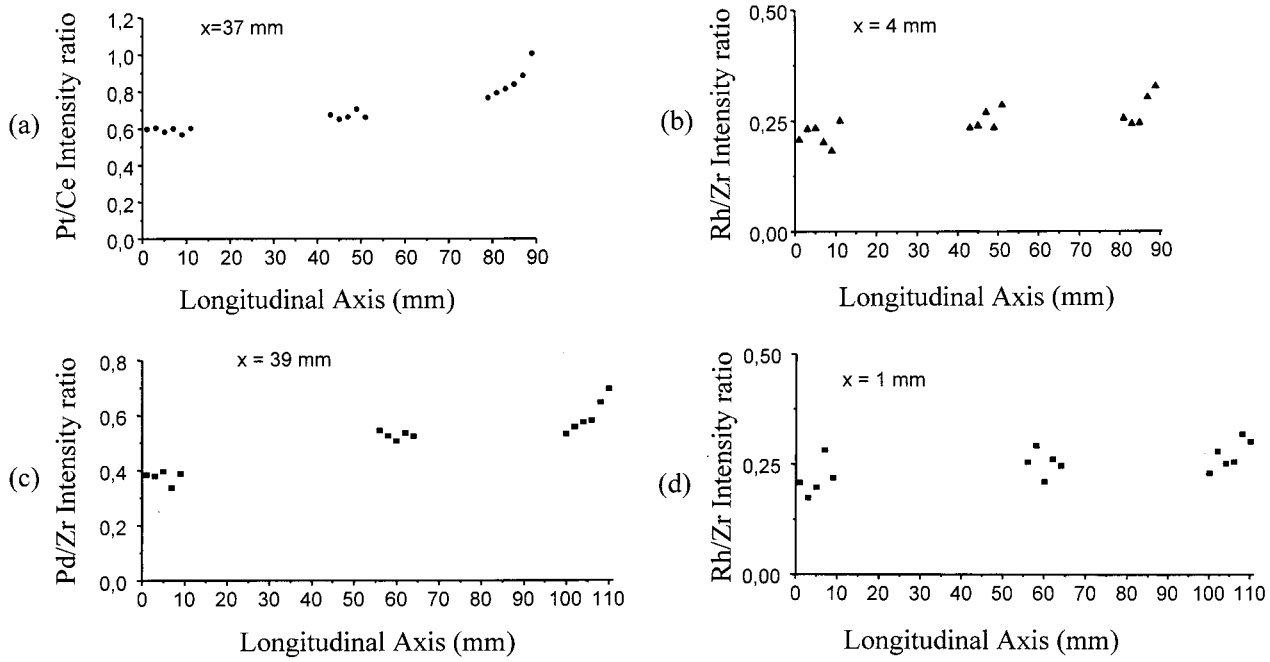

Figure 9. Lateral profiles of (a) Pt and (b) Rh in the front substrate and (c) Pd and (d) Rh in the rear substrate. The profiles have an "*x*" fixed longitudinal location.

and c). The Rh content in both the front and rear substrates seems to be more uniform (Figure 9b and d). The radial variability of intensities for the three elements is in the range 5−12% relative standard deviation in the sampling locations.

CONCLUSIONS

LIBS has been proved to be a feasible approach for the distribution analysis of PGM in automobile catalytic converters, and it has been demonstrated to work quite well for the converters even with as a weak structure as the intact washcoat. Because of the loose nature of the washcoat, the lateral and depth resolution is limited by the large craters formed by the focused laser beam. Consequently, there are difficulties when dealing with typical problems in deactivation of converters such as sintering or dispersion of elemental constituents in a submicrometric scale. Nevertheless, the capability of LIBS to work with large structures with minimum sample preparation is of great interest for this application and it is ideally suited to follow the release of the PGM as a result of engine operation. Although the detection power of LIBS is limited, it has been proved sufficient for detection of the PGM at least in the fresh catalyst. Work is in progress on aging catalytic converters and subsequent LIBS analysis to study the effect of engine regime on the extent of PGM release.

ACKNOWLEDGMENT

This work has been supported by the European Union under Contract CEPLACA, ENV4-CT97-0518. The authors are grateful to Prof. J. Pascual for the Rutherford backscattering data.

Received for review March 19, 1999. Accepted July 7, 1999.

AC9902998